J. Electroanal. Chem., 306 (1991) 87–109
Elsevier Sequoia S.A., Lausanne

The application of rapid scan cyclic voltammetry and digital simulation to the study of the mechanism of diphenylamine oxidation, radical cation dimerization, and polymerization in acetonitrile

Hongjun Yang and Allen J. Bard

Department of Chemistry, The University of Texas at Austin, Austin, TX 78712 (USA)

(Received 18 September 1990; in revised form 19 November 1990)

Abstract

Cyclic voltammetry, performed with ultramicrodisk electrodes, was used to investigate the mechanism of the initial step of the electropolymerization of diphenylamine in acetonitrile. The $Ph_2NH^{\cdot+}$ radical cations were electrochemically detected at scan rates above 100 V/s. Initially, the electrogenerated $Ph_2NH^{\cdot+}$ radical cations undergo a second-order radical cation–radical cation coupling reaction to form diphenylbenzidine. Digital simulations of the voltammograms suggest the reaction occurs by an initial dimerization of the radical cations, followed by proton loss and additional electron transfer reactions (an EC_2EE-type of mechanism). A rate constant of 2.0 ($\pm$0.5)$\times 10^5$ M^{-1} s^{-1} for the radical cation coupling reaction was determined. Deprotonation associated with the coupling depends upon the water content. A new criterion for distinguishing among different mechanisms of following chemical reactions by cyclic voltammetry, based on changes in peak shape, is proposed.

INTRODUCTION

The electrochemical oxidation of aromatic amines occurs readily in both aqueous and nonaqueous media. Indeed, there have been a large number of studies of these electrode reactions [1,2], and the oxidation of molecules like aniline and triphenylamine served as model reactions in the study of electrochemical methods for elucidating electrode reaction mechanisms [3,4]. Renewed interest in the electrochemistry of aromatic amines in recent years is associated with the fabrication of electronically conductive polymers, such as polyaniline [5–8]. Electropolymerization is an effective method for preparing these materials, and electrochemical methods are useful in characterizing them. While many papers have been published dealing with the preparation of polymeric materials, their properties, and their utilization, only sparse consideration has been given to the mechanism of the dimerization and

0022-0728/91/$03.50

polymerization reactions [7–16,21] and few have provided experimental results to support the proposed mechanism [17,18,21]. The difficulty of resolving the detailed mechanism is due to the fast rates of the homogeneous chemical reactions that follow the initial electron transfer at the electrode surface. A reasonable mechanism for the initial step of electropolymerization is that the radical cations obtained upon electrochemical oxidation undergo a rapid radical-radical coupling reaction with associated deprotonation to produce the dimer. The dimer is further oxidized by loss of one or two electrons [2,17–21]. An alternative mechanism would involve initial coupling of the radical cation with the parent molecule, followed by subsequent electron and proton transfer reactions [2,21,22]. These mechanisms are analogous to those studied some time ago in connection with reductive hydrodimerization reactions of activated olefins [23]. However, these proposed mechanisms are difficult to verify, because the initial radical cations have not been detected in most cases. Therefore, the mechanism of the initial stage in the polymerization of aromatic amines has remained an unsettled question.

We discuss here the electrochemical oxidation of diphenylamine in acetonitrile (MeCN) solutions. We show that digital simulations of rapid scan cyclic voltammograms obtained with an ultramicroelectrode suggest the reaction mechanism follows an initial dimerization of the radical cations followed by proton loss and additional electron transfer reactions (an EC_2EE-type process [24]). These steps are presumably followed by additional reactions that lead to the polymer, poly(diphenylamine). This polymer has been synthesized chemically and electrochemically in both aqueous and non-aqueous solutions [20,25–27], and its conductivity, electrochemical stoichiometry, and other properties examined. In one of these studies the reaction scheme proposed involved reaction of the radical cation with a molecule of diphenylamine to produce a dimer [25]. However, the other proposed a radical–radical reaction scheme [20]. Gray and Dao showed that diphenylamine followed a 4,4′ C–C phenyl–phenyl coupling during its electrodimerization [27].

EXPERIMENTAL

The ultramicroelectrodes were prepared by sealing Pt wires of different diameters (5, 10, 25, 50, 100 μm) in 1 mm i.d. Pyrex capillary. The electrical connection was made with silver paint. The electrodes were polished with 1 μm, followed by 0.5 μm, diamond paste (Buehler Ltd., Lake Bluff, IL), cleaned by sonication in 30% HNO_3, rinsed in water, and dried before use.

A single compartment vacuum-line electrochemical cell was employed, in which an isolated silver wire quasi-reference electrode (AgQRE) was placed in the center and surrounded by five working electrodes of different sizes and a Pt flag counter electrode (Fig. 1). Potentials are reported here vs. the AgQRE, which in turn was calibrated against the ferrocene/ferrocenium (Fc/Fc^+) couple.

Acetonitrile (spectrophotometric grade, Mallinckrodt Inc., Paris, KY) was purified by drying with calcium hydride, followed by two distillations from phosphorus pentoxide and a third distillation from calcium hydride. Tetrabutylammonium

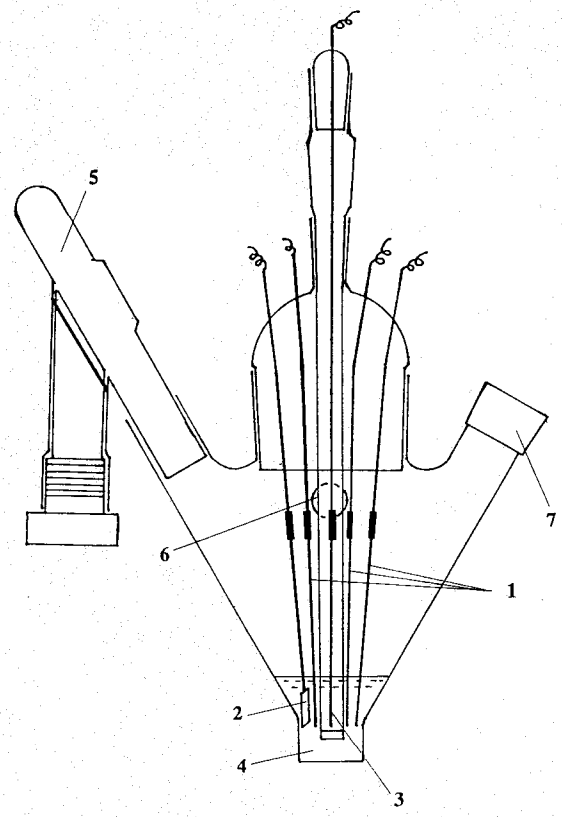

Fig. 1. A single compartment cell with five working microelectrodes. (1) Working electrodes (UME), (2) counter electrode, (3) reference electrode (Ag-QRE), (4) solution, (5) sample reservoir, (6) to vacuum line, (7) rubber septum.

hexafluorophosphate, $TBAPF_6$ (Southwestern Analytical Chemicals, Austin, TX), the supporting electrolyte, was recrystallized twice from ethanol and acetone. Diphenylbenzidine (Aldrich Chemical Company, Inc., Milwaukee, WI) and other chemicals were used as received. Vanlube 81 (Vanderbilt Chemicals, Norwalk, CT) was crystallized twice from ethanol.

Before each voltammetry experiment the amount of $TBAPF_6$ supporting electrolyte to yield a concentration of 0.1 M and ca. 0.4 g ICN Alumina N-Super 1 (ICN Biomedicals Inc., Costa Mesa, CA) were added to the cell, which was attached to the vacuum line. Prior to the distillation of the MeCN the cell was heated at 90 °C under vacuum ($\sim 10^{-5}$ Torr) for ca. 10 h. Diphenylamine had been added to a side arm of the cell in the dry box and was not heated to avoid sublimation. The concentrations of diphenylamine ranged from 0.5 to 5 mM. MeCN (10 ml) was distilled into the cell on the vacuum line, then the diphenylamine was added to the solution in the cell.

Electrochemical measurements were performed with a home-built bipotentiostat (sensitivity of 0.1 μA/V and response of 100 kHz). A PAR model 175 universal programmer (Princeton Applied Research Corp., Princeton, NJ) served as a signal generator. The cyclic voltammograms at scan rates less than 1 V/s were recorded with an X–Y recorder. At other scan rates, the voltammograms and steady-state currents were recorded with a Norland digital oscilloscope, model 3001 (Norland Corp., Fort Atkinson, WI) with a minimum acquisition time of 2 μs/point. All experiments were performed with the cell held in a Faraday cage.

RESULTS AND DISCUSSION

Cyclic voltammetry

A typical cyclic voltammogram of diphenylamine, Ph_2NH, obtained at a Pt disk (0.5 mm diam.) electrode in anhydrous MeCN solution containing 0.1 M $TBAPF_6$ is shown in Fig. 2. In the first scan to positive potentials at $v = 0.2$ V/s, the anodic peak, I, corresponding to the oxidation of Ph_2NH monomer, appeared at ca. 0.90 V vs. AgQRE. The AgQRE potential was calibrated vs. the Fc/Fc^+ couple by adding ferrocene solution to the cell. Since the standard potential of the Fc/Fc^+ couple is

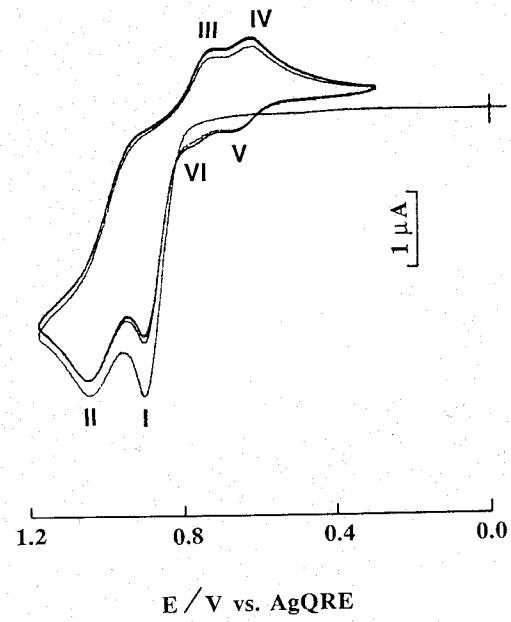

Fig. 2. Cyclic voltammogram of 2.36 mM diphenylamine in acetonitrile containing 0.1 M $TBAPF_6$ at Pt disk electrode ($d = 0.5$ mm), scan rate = 0.2 V/s.

usually given as 0.307 V vs. an aq. SCE [24], the potential of peak I at this scan rate is 0.83 V vs. aq. SCE. After peak I, in very dry MeCN, a second broader peak, II, appeared at more positive potentials. As shown below, this peak results from the oxidation of the protonated Ph_2NH monomer, $Ph_2NH_2^+$. Note that peak II was observed only in very dry MeCN [28]. Upon scan reversal no cathodic peaks corresponding to anodic peaks I and II were found at this scan rate. This indicated that the electrogenerated radical cations, e.g., $Ph_2NH^{\cdot+}$, were completely consumed in following chemical reactions. However, two well-defined cathodic peaks, III and IV, appeared at ca. 0.74 V and 0.62 V (0.67 V and 0.55 V vs. SCE). In the second positive potential scan, two new anodic peaks, V and VI, were observed; these correspond to cathodic peaks IV and III, respectively. Peak VI was not very clear, because it merged with peak I, but at higher scan rates, peak VI grew into a distinct wave. The peak potential separations, ΔE_p, for III/VI and IV/V were both about 60 mV. Thus, these peaks are characteristic of nernstian redox couples. Upon repeated scans, the height of peak I, $i_{pa(I)}$, decreased while those of peaks III to VI increased.

As a guide to the experiments and results that follow, we present here the proposed mechanism for the electrode reaction [29,30].

$$Ph_2NH - e^- \rightleftharpoons Ph_2NH^{\cdot+} \qquad \text{(wave I)} \qquad (1')$$

$$2\ Ph_2NH^{\cdot+} \xrightarrow{k} (Ph_2N)_2 + 2\ H^+ \qquad (2')$$

$$(Ph_2N)_2 - e^- \rightleftharpoons (Ph_2N)_2^+ \qquad \text{(waves IV/V)} \qquad (3')$$

$$(Ph_2N)_2^+ - e^- \rightleftharpoons (Ph_2N)_2^{2+} \qquad \text{(waves III/VI)} \qquad (4')$$

where $(Ph_2N)_2$ will be shown to be *N,N′*-diphenylbenzidine (DPB). This scheme generally follows that of other aromatic amines, e.g., *N,N*-dimethylaniline, where *N,N,N′,N′*-tetramethylbenzidine (TMB) is formed as a dimerization product [9,31,32].

Identification of the dimerization product as DPB

In reaction (2′) we show formation of the dimer by reaction of two $Ph_2NH^{\cdot+}$ radical cations. As discussed below, we favor this scheme to the alternative path involving reaction of a $Ph_2NH^{\cdot+}$ radical cation with one parent monomer, followed by loss of another electron. The radical cations can couple in different ways [22,28], e.g., C–C, C–N, and N–N, to afford different dimerization products. These products have different structures, which can be distinguished by their characteristic redox behavior in cyclic voltammograms.

The cyclic voltammogram of an authentic sample of *N,N′*-diphenylbenzidine (DPB) is shown in Fig. 3a. Two reversible redox waves are apparent in both anodic and cathodic scans. The potential potentials are identical to those for peaks III/VI and IV/V of Ph_2NH given in Fig. 2. We thus propose that DPB is the only dimerization product. This is in good agreement with FTIR spectroscopic results that show that diphenylamine in MeCN undergoes a 4,4′ C–C phenyl–phenyl

coupling pathway [27]. Thus reactions (1′) to (4′) can be rewritten more explicitly as follows:

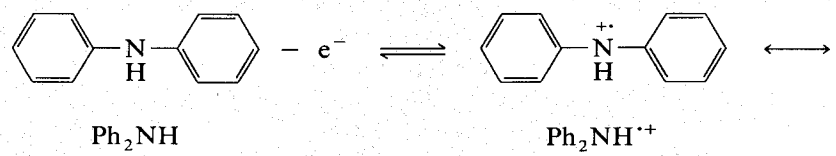

Ph_2NH $Ph_2NH^{\cdot+}$

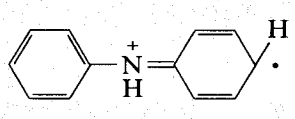

(1)

$Ph_2NH^{\cdot+}$

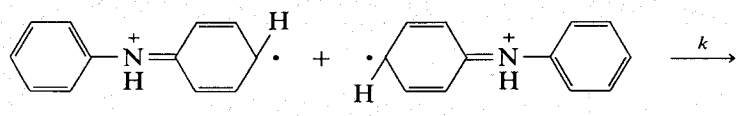

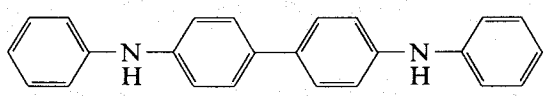

(2)

DPB

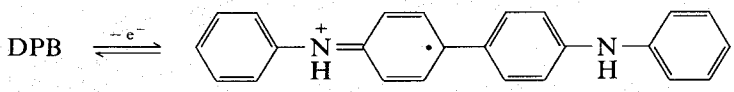

(3)

DPB^+

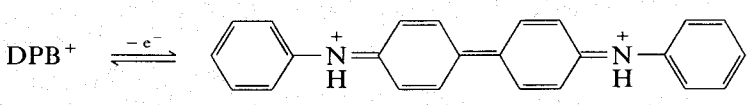

(4)

During repetitive scanning of a solution containing only DPB, the peak currents did not show appreciable changes, indicating that DPB and its oxidation products do not undergo electropolymerization reactions. If Ph_2NH was added to that solution and the upper switching potential was set at 0.80 V, i.e., just before the start of the oxidation of Ph_2NH, the peak current still did not change upon cycling (Fig. 3b). When the switching potential was changed to 1.2 V, the cyclic voltammogram obtained (Fig. 3c) was similar to Fig. 2. However, in this instance, the peak currents attributed to DPB increased, due to the augmentation of the original current by that due to the DPB generated by dimerization of Ph_2NH. Furthermore,

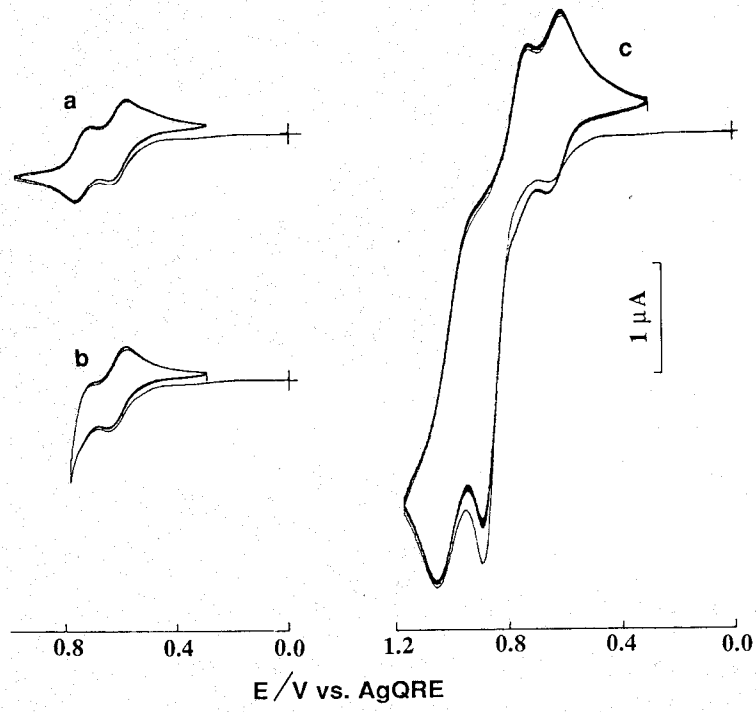

Fig. 3. Cyclic voltammograms of (a) 0.51 mM diphenylbenzidine; (b), (c) with the addition of 2.84 Ph_2NH, in MeCN solution of 0.1 M $TBAPF_6$ at Pt disk electrode $d = 0.5$ mm), scan rate = 0.1 V/s.

the peak current increased as the scan continued, which suggested that adding DPB into Ph_2NH solution might contribute to the electropolymerization of Ph_2NH.

The cyclic voltammogram of the amine Vanlube 81 in MeCN (Fig. 4) shows a reversible oxidation. Blockage of the para-position of the phenyl ring with the bulky hydrocarbon group prevents C–C coupling. This implies that the coupling occurs in the para-position, with little tendency to couple in the ortho-position. The reversibility of this reaction suggests that the radical cation is stable during the scans and does not undergo a deprotonation reaction, e.g., by transfer of a proton to parent amine.

Effect of radical cation deprotonation

The total number of electrons passed in the overall oxidation reaction per molecule of Ph_2NH, n_{app}, depends upon the occurrence of proton transfer reactions of $Ph_2NH^{\cdot+}$. The overall dimerization of the electrogenerated $Ph_2NH^{\cdot+}$ radical cations is associated with deprotonation [17,18,28–30,33]. In Ph_2NH solution,

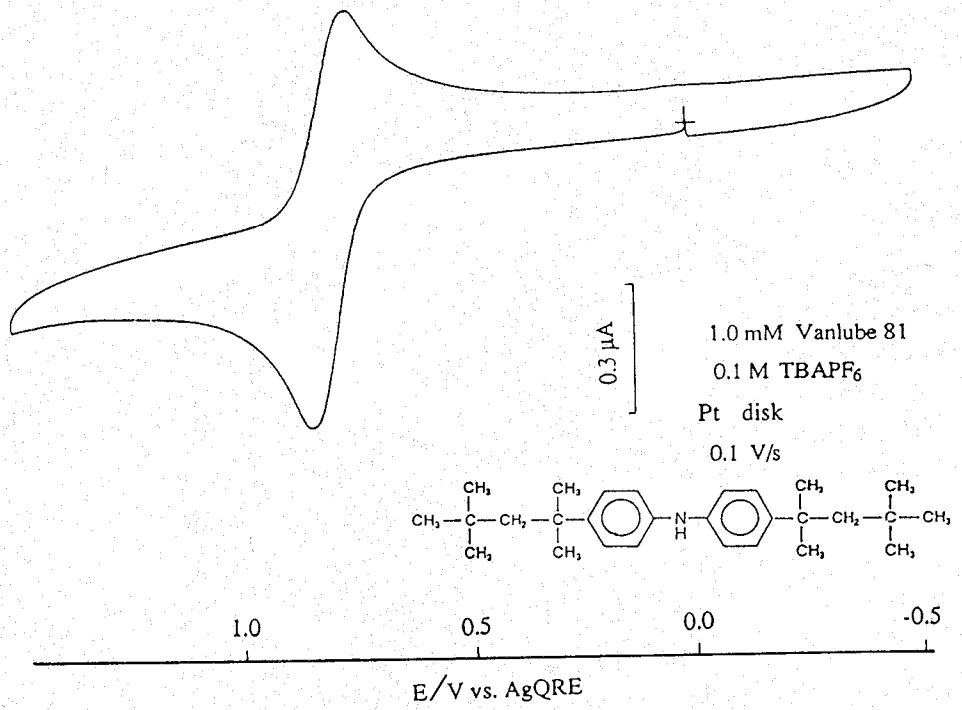

Fig. 4. Cyclic voltammogram of 1.0 mM Vanlube 81 in 0.1 M $TBAPF_6$ MeCN solution.

Ph_2NH itself is the best proton acceptor. Given this possibility, and the presence of peak II, reaction (2) should be rewritten as

$$2\ Ph_2NH^{\cdot+} + 2\ Ph_2NH \xrightarrow{k_s} DPB + 2\ Ph_2NH_2^+ \tag{5}$$

Under these conditions, the overall reaction [summing reactions (1), (5), (3), (4)] is

$$4\ Ph_2NH - 4\ e^- \rightarrow DPB^{2+} + 2\ Ph_2NH_2^+ \tag{6a}$$

and one electron is lost per Ph_2NH monomer, i.e., $n_{app} = 1$. This can be compared to the overall reaction summing (1) through (4) where

$$2\ Ph_2NH - 4\ e^- \rightarrow DPB^{2+} + 2\ H^+ \tag{6b}$$

and $n_{app} = 2$. As described below, the mechanism of the reaction was probed by investigating the effect of concentration, c, and scan rate, v, on the height of the first wave. The intervention of the $n_{app} = 1$ route described above would make this mode of diagnosis much less useful. In using n_{app} to study the reaction, one looks at the extent of occurrence of reaction (2) during the scan [i.e., considers the dimensionless parameter $k_2c/v(RT/F)$]. When this is small, $n_{app} \rightarrow 1$; when it is large $n_{app} \rightarrow 2$ [in the absence of protonation of Ph_2NH, reaction (5)], because oxidation of DPB to DPB^{2+} [reactions (3) and (4)] occurs at the potential of the first anodic

wave. Thus if x is the fraction of Ph_2NH^+ converted to DPB during the scan, then the overall reaction in that time period is

$$Ph_2NH - (1+x)\ e^- \rightarrow (x/2)\ DPB^{2+} + (1-x)\ Ph_2NH^{\cdot+} + H^+ \quad (7)$$

and $n_{app} = 1 + x$. However if the free protons in reaction (7) are scavenged by parent Ph_2NH, the overall reaction becomes

$$(1+x)\ Ph_2NH - (1+x)\ e^- \rightarrow (x/2)\ DPB^{2+} + (1-x)\ Ph_2NH^{\cdot+} + x\ Ph_2NH_2^+ \quad (8)$$

In this case $n_{app} = 1$, independent of x. If all of the $Ph_2NH^{+\cdot}$ were deprotonated, n_{app} would equal $2/(1+x)$. Clearly the intervention of protonation reactions of Ph_2NH complicates the interpretation of the CV behavior in terms of the reaction mechanism.

To investigate whether Ph_2NH was controlling the proton transfer reactions, we studied the effect of addition of pyridine (Py) (a stronger base than Ph_2NH) and H_2O on the CV behavior. In the presence of Py, n_{app} should equal 2, since the overall reaction would be

$$2\ Ph_2NH + 2\ Py - 4\ e^- \xrightarrow{k} DPB^{2+} + 2\ PyH^+ \quad (9)$$

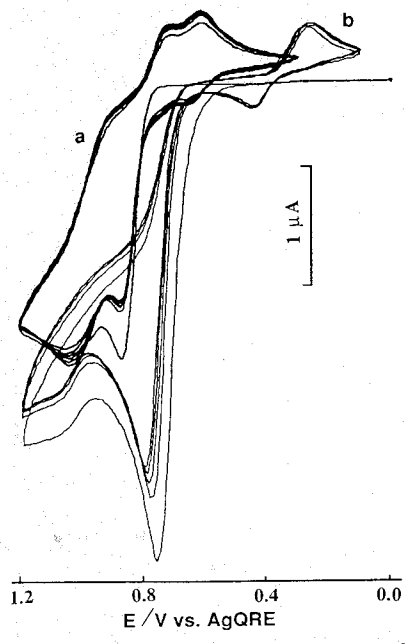

Fig. 5. Cyclic voltammograms of 2.01 mM Ph_2NH in MeCN containing 0.1 M $TBAPF_6$ at Pt disk electrode ($d = 0.5$ mm), scan rate = 0.1 V/s, (a) without; (b) with the addition of 5 μl pyridine.

The CV upon the addition of 5 μl pyridine (ca. 6.2 mM) is shown in Fig. 5. The peak current of the first anodic peak increased to almost twice that of the pyridine-free solution, and shifted to less positive potentials by about 120 mV. Moreover, the redox behavior of the products on scan reversal changed. Thus the addition of Py changes the route of electrooxidation of Ph_2NH, probably via deprotonation of $Ph_2NH^{\cdot+}$ and causes the onset of a different reaction sequence. It is known that the coupling products of aromatic amine oxidation depend upon the acidity or basicity of the medium [28]. The course of this reaction was not investigated further.

The occurrence of peak II, ascribed to the oxidation of $Ph_2NH_2^+$ in very dry MeCN, suggests that this species arises from protonation of Ph_2NH by protons produced in the overall dimerization reaction. As the scan rate increased, peak II decreased and eventually disappeared, suggesting that protonation of Ph_2NH by $Ph_2NH^{\cdot+}$ directly was not significant. However peak II was not seen in an earlier study of Ph_2NH in MeCN at similar scan rates, suggesting that small amounts of water in the MeCN can participate in the reaction sequence. Figure 6 shows the effect of adding 0.1% (by volume) water to the dry MeCN solution. Peak II disappeared, while the peak current of peak I increased to twice its original value at

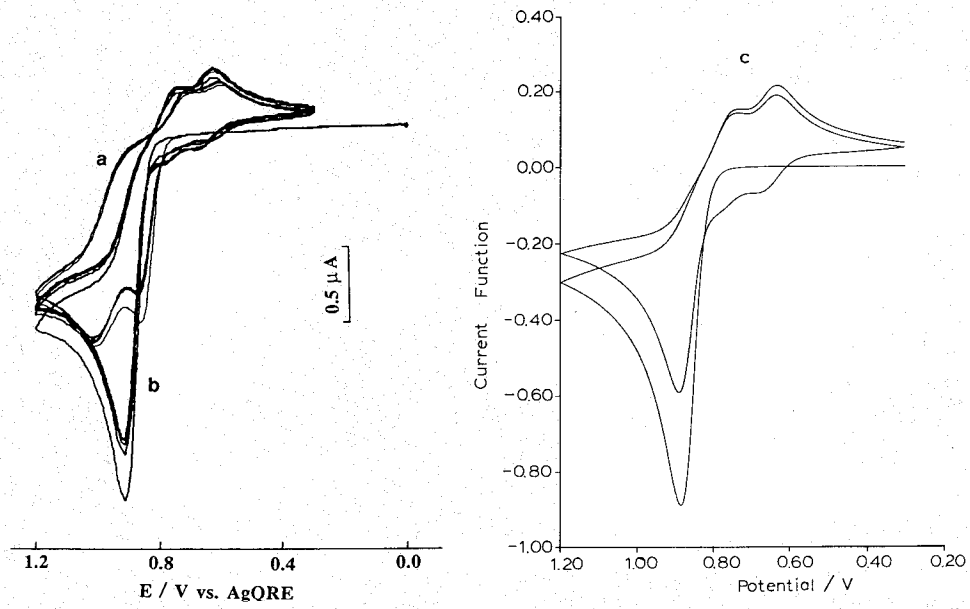

Fig. 6. Cyclic voltammograms of 1.42 mM Ph_2NH in MeCN containing 0.1 M $TBAPF_6$ at Pt disk electrode ($d = 0.5$ mm), scan rate $= 0.1$ V/s, (a) without; (b) with the addition of 10 μl water; (c) simulated voltammogram with $k = 2.0 \times 10^5$ M^{-1} s^{-1}, $D = 2.5 \times 10^{-5}$ cm^2 s^{-1}, all other parameters taken with real values.

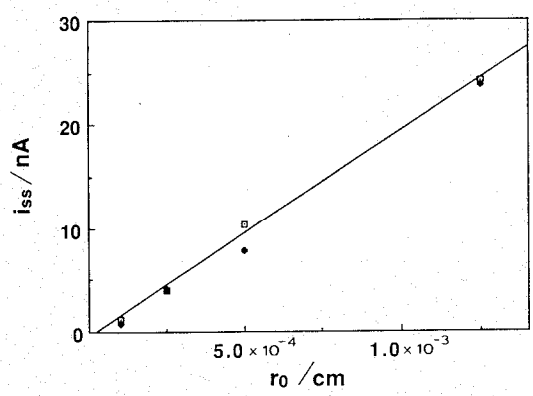

Fig. 7. Plot of steady-state current vs. radius of microdisk electrodes. 1.04 mM Ph_2NH in MeCN solution of 0.1 M $TBAPF_6$ (and 0.1% H_2O).

this scan rate. All peak potentials were slightly shifted by about 25 mV in the positive direction. This is probably due to the effect of water on the potential of the AgQRE. The relative height of waves III to VI essentially did not change. Thus the slightly wet MeCN system is better for a mechanistic study, since water displaces Ph_2NH as the proton acceptor and allows n_{app} to be identified solely with the dimerization reaction, as discussed above. This simplifies the CV study and allows the variation of n_{app} between 1 and 2 as a function of c and v to be used to probe the reaction mechanism.

Diffusion coefficient of Ph_2NH

Voltammetry at an ultramicroelectrode (UME) was used to determine the diffusion coefficient of Ph_2NH in MeCN containing 0.1% water. The steady-state current at an ultramicrodisk electrode is $i_{ss} = 4nFDcr_0$ [34–37] where c is the bulk concentration of the electroactive species, D is its diffusion coefficient, r_0 is the radius of the disk, and n is the number of electrons involved in the electrode reaction [34–37]. This measurement was made at steady-state conditions, where the dimerization reaction is essentially complete and $n = n_{app} \approx 2$ with several different UMEs with r_0's of 1–12.5 μm (Fig. 7). From the slope of the plot of steady-state current vs. r_0, the diffusion coefficient of Ph_2NH was found to be 2.5×10^{-5} cm^2/s. This value is approximately one half that previously reported, based on disk electrode measurements with the assumption that $n = 1$ [25].

Radical cation-radical cation coupling vs. radical cation–parent coupling in the dimerization reaction

The clear presence of dimerization product and the variation of n_{app} shows that the reaction at wave I can be described as an EC_2E type process [reactions (1) to (4)]. However, the nature of the dimerization reaction remains to be resolved. Two pathways are possible. In the first case, as shown in reaction (2), two radical cations

couple. Another possibility is the ECEEE route; reaction (1) followed by coupling of the radical cation with parent:

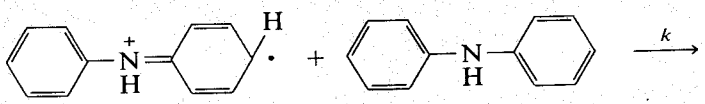

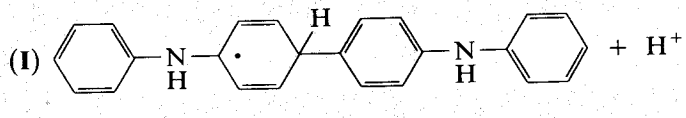

(10)

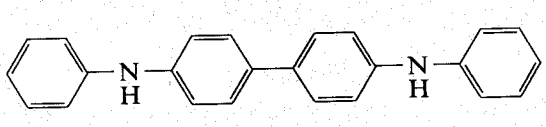

(11)

DPB

in which a radical cation couples with a parent monomer, followed by reactions (3) and (4) [22].

Many techniques are available for elucidating reaction mechanisms [24,38–40]. For the reaction under consideration here, techniques that depend primarily on reversal and detection of $Ph_2NH^{\cdot+}$, e.g., double potential step chronoamperometry, are less useful, both because the following reaction of Ph_2NH^+ is fast and because the closeness of the wave III/VI pair restricts the potentials where the reverse process ($Ph_2NH^{\cdot+}$ reduction) can be studied uncomplicated by reduction of DMB^+ and DMB^{2+}. Thus we have studied the reaction by CV, and utilized the change in the forward parameter [24] (i.e., $i_{pa(I)}$ or n_{app}) and the shape of the CV wave, which turns out to be a particularly useful diagnostic criterion in this case for distinguishing between the dimerization routes. The study was carried out with ultramicroelectrodes, so that, as discussed in previous papers [37,41–44], fast scan rates can be utilized to bring the characteristic measurement time into a region where kinetic effects could be revealed. To allow studies over the full range of behavior and with different concentrations, this involved variation of v over a range of almost 5 orders of magnitude. This, however, requires the use of several different UMEs with different r_0-values. To carry out kinetic studies at an UME, it is most convenient to work under conditions where linear diffusion is obtained. This requires that the relevant dimensionless parameter $D/r_0^2\ v(F/RT)$ be small (e.g., < 0.25). At larger values of this parameter (i.e., at smaller values of r_0 and v) hemispherical contributions to diffusion become significant. However, to be in a kinetically useful region for study of the dimerization reaction, the dimensionless parameter $kc/v(F/RT)$ must be in an appropriate range, e.g., roughly between 0.1 and 10. Thus UMEs of

several different radii (2.5 μm to 0.25 mm) were employed in this study over a range of values of v and c.

High scan rates ($\geqslant$ 100 V/s) were needed to see a reversal wave attributable to reduction of $Ph_2NH^{\cdot+}$. At 100 V/s (Fig. 8a) a very small reduction wave is observed on scan reversal, but waves for the dimerization products (III/VI and IV/V) are still prominent. However at a scan rate of 10^4 V/s (Fig. 9), these DMB-based waves are almost gone on the first scan, and the $Ph_2NH/Ph_2NH^{\cdot+}$ couple yields an almost Nernstian response (distorted, however, by charging current and some uncompensated iR-drop). However on continued scanning one could still observe two reversible one-electron transfer waves of the DPB species. These results suggest kc for the dimerization reaction is of the order of 10^3 s^{-1}.

In considering the dimerization reaction, one must consider the coupling mode (i.e., C–C vs. C–N) and the reaction sequence. Radical cation–parent coupling [as shown in eqn. (10)] has been described in terms of a C–N coupling reaction [10,30]. However we see no evidence of a C–N coupled product. As discussed earlier, the CV results suggest that the dimerization product is DPB, a para C–C coupled compound. Oxidation of the intermediate I probably would occur at potentials of wave I, in the ECE sequence suggested by reactions (1), (10), and (11). Under these conditions the radical cation $Ph_2NH^{\cdot+}$ would also be capable of oxidizing **I** by a DISP [22,45,46] route

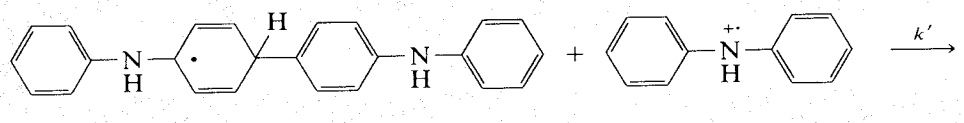

(**I**)

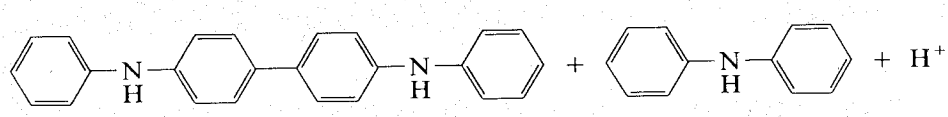

DPB $\qquad\qquad$ Ph_2NH

(12)

In this route Ph_2NH, is regenerated. Hence, there are three types of mechanisms:

(A) Radical ion–radical ion (R–R) coupling, via eqns. (1), (2), (3), and (4) (DIM).

(B) Radical ion-parent (R–P) coupling followed by electron transfer, eqns. (1), (10), (11), (3), and (4) (ECE).

(C) Radical ion-parent coupling followed by disproportionation, eqns. (1), (10), (11), (12), (3), and (4) (DISP).

All of these ultimately lead to the same product, DMB^{2+}, and would show a variation of n_{app} between 1 and 2 in the appropriate range of v and c. However the detailed shape for this variation with $k_2c/v(RT/F)$ depends upon whether mechanism A, B, or C was followed.

To establish the theoretical working curves, digital simulations [24] of the

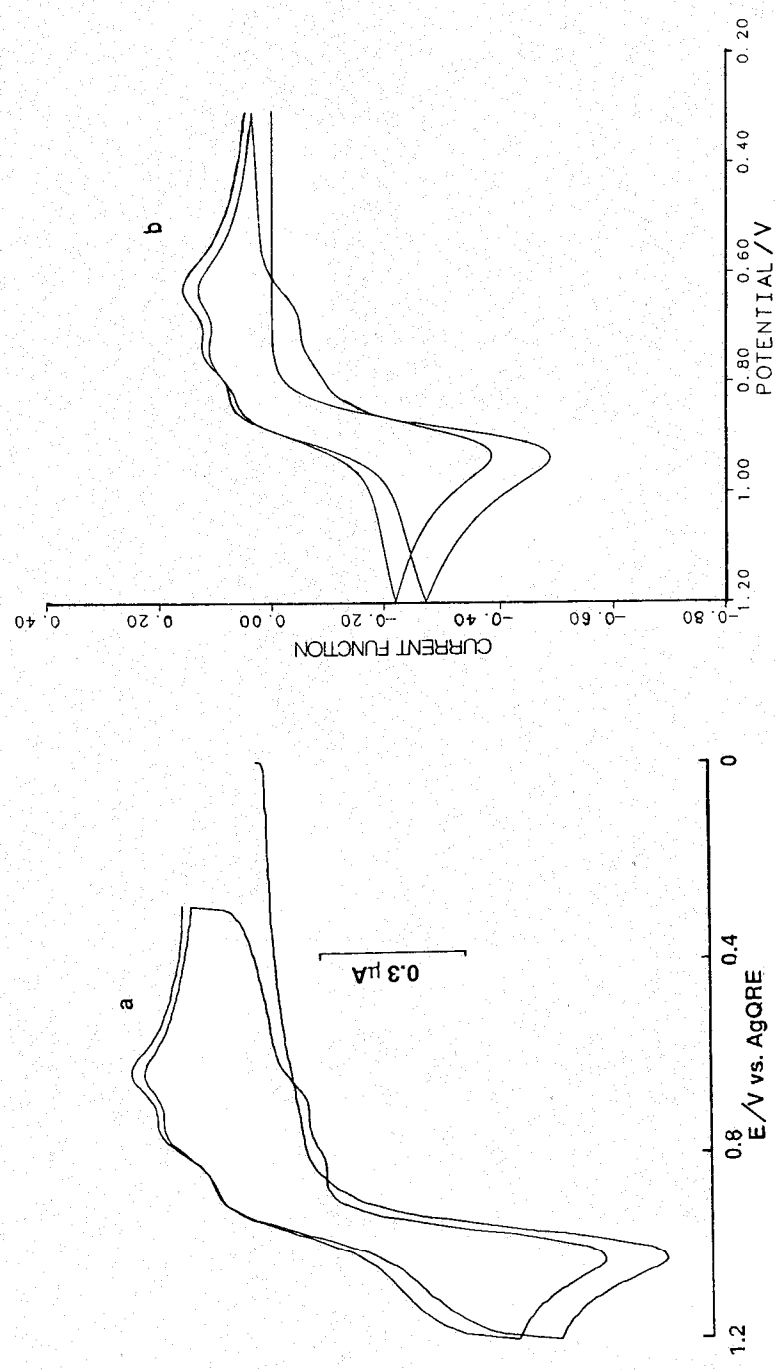

Fig. 8. Cyclic voltammogram of (a) 2.36 mM Ph_2NH in MeCN solution of 0.1 M $TBAPF_6$ (and 0.1% H_2O) at Pt microelectrode ($d = 50$ μm), scan rate = 100 V/s, (b) simulated voltammogram with $k = 2.0 \times 10^5$ M^{-1} s^{-1}, $D = 2.5 \times 10^{-5}$ cm^2 s^{-1}, all other parameters taken with real values.

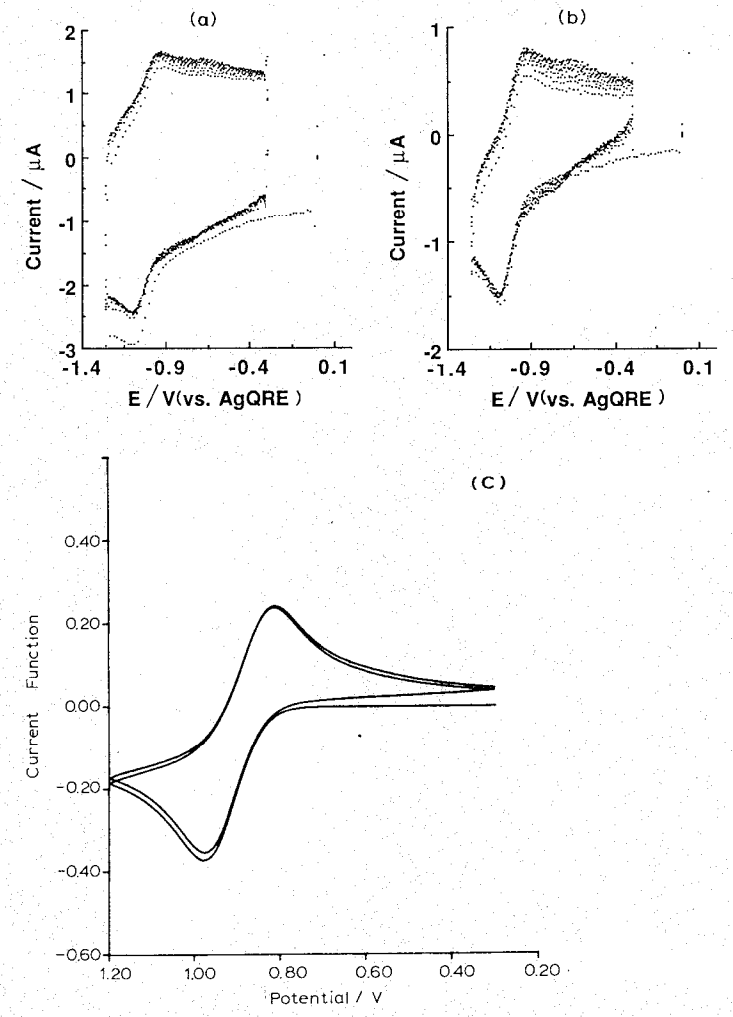

Fig. 9. Cyclic voltammogram of (a) 3.90 mM Ph_2NH in MeCN solution of 0.1 M $TBAPF_6$ (and 0.1% H_2O) at Pt microelectrode ($d = 0.005$ mm), scan rate = 10000 V/s, (b) after subtracting the charging current background, (c) simulated voltammogram with $k = 2.0 \times 10^5$ M^{-1} s^{-1}, $D = 2.5 \times 10^{-5}$ cm^2 s^{-1}, all other parameters taken with real values.

different mechanisms were carried out (see Appendix). The heterogeneous electron transfer reactions were assumed to be rapid, with $k°$-values of 1.0 cm/s and $\alpha = 0.5$. As shown below, we favor the route given by mechanism A. Individual cyclic voltammograms simulated by this mechanism were in good agreement with the experimental ones (see Figs. 6, 8, 9). The simulated voltammograms with different values of k and k' were also used to prepare a plot of the current function ($i_p/v^{1/2}c$) or n_{app} against c/v (Fig. 10).

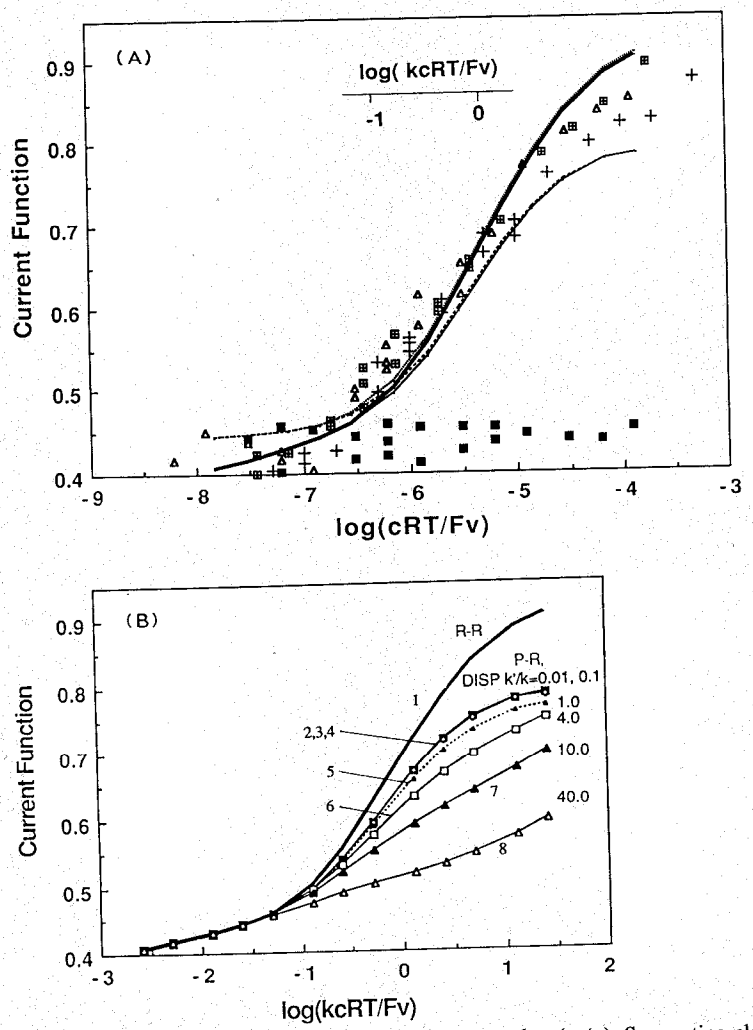

Fig. 10. (A) Normalized current of the first peak vs. log (c/v). Supporting electrolyte: 0.1 M $TBAPF_6$. Ph_2NH concentration: (⊞) 1.42 mM, (△) 2.36 mM, (+) 3.90 mM with 0.1% H_2O, (■) 2.36 mM without added H_2O. Lines: simulated working curves for different proposed mechanisms: (———) R–R coupling, $k^\circ = 1.0$ cm/s; (· · · · ·) $k^\circ = 1.0 \times 10^{10}$ cm/s, $k = 10^6$ M^{-1} s^{-1}; (———) P–R coupling, $k^\circ = 1.0$ cm/s; (— — —) $k^\circ = 1.0 \times 10^{10}$ cm/s, $k = 10^6$ M^{-1} s^{-1}. (B) Simulated working curve for the cases in which disproportionation reaction is involved (curves 3–8) with different ratios of $k'/k = 0.01$, 0.1, 1.0, 4.0, 10.0, 40.0, respectively, compared to R–R (1) and P–R (2) routes.

In Fig. 10B, curve 1 pertains to mechanism A, curve 2 to B, and curves 3–8 to mechanism C with $k'/k = 0.1$ to 40.0, respectively. In the case of mechanism C, eqns. (11) and (12) occur in parallel, with both in series with eqn. (10). Therefore, in most cases, the rate of the reaction in eqn. (10) controls the behavior. If k' is small, the reaction in eqn. (12) does not make a significant contribution to the first

oxidation peak current. When k' becomes larger, eqn. (11) makes a smaller contribution to the oxidation current, resulting in a decrease in n_{app}.

Figure 10A shows that the experimental data show a better fit to mechanism A. The rate constant of 2.0 (± 0.5) $\times 10^5$ M^{-1} s^{-1} for the radical–radical coupling pattern was obtained by matching the normalized currents of the first peak in CV at different scan rates with the simulated working curve. Examination of the simulated cyclic voltammograms also showed that the shape of the oxidation wave was different for the different mechanisms. Thus the difference between the peak potential (E_p) and the potential at half the peak height ($E_{p/2}$) was a useful diagnostic criterion for distinguishing among paths A, B, and C. While such an approach is often used in studies of heterogeneous electron transfer kinetics [38–40], and shifts of E_p with v and c are widely employed in studies of homogeneous reactions [45,46], we are unaware of any previous studies involving $E_p - E_{p/2}$ measurements in mechanistic studies.

Results for $E_p - E_{p/2}$ vs. $kc/v(RT/F)$ from the simulated voltammograms are given in Fig. 11 for mechanisms A and B. At small values of the dimensionless parameter (small kc or large v) the values approach the expected nernstian value of 58 mV (25 °c); The deviations towards larger values at very small values of the dimensionless parameter reflect the effects of very large scan rates with a fast, but finite, heterogeneous electron transfer rate constant (1 cm/s). At smaller values of kc/v, the waves for mechanism A sharpen much more than those for B. This can be understood qualitatively as follows. For B, (R–P coupling) the concentrations of R and P decrease simultaneously, so the potential, governed largely by the Nernst equation involving R and P, is not greatly perturbed compared to the uncomplicated case. However in A, with R–R coupling, the concentration of R is decreased much

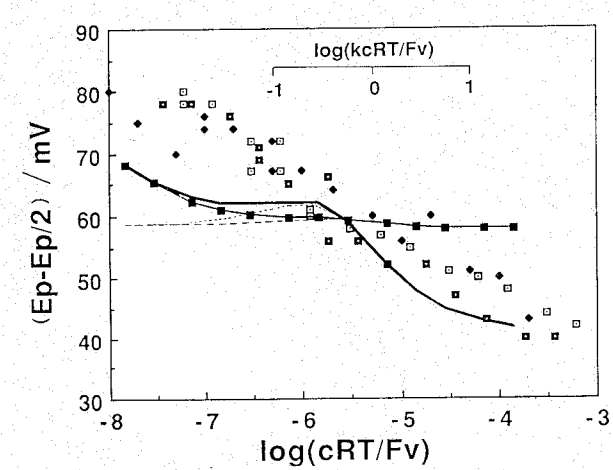

Fig. 11. Variation of ($E_p - E_{p/2}$) vs. log λ. Ph_2NH concentration: (■) 1.42 mM; (⊡) 2.36 mM; (◆) 3.90 mM. Solid lines are simulation results with $k^\circ = 1.0$ cm/s; dashed lines are $k^\circ = 1.0 \times 10^{10}$ cm/s (———) R–R, (■———■) P–R.

more extensively than P. The experimental results shown in Fig. 11 at $kc/v(F/RT)$ above 1 clearly favor the R–R route. The deviations at small values of $kc/v(F/RT)$ probably represent mainly the effect of uncompensated resistance on the experimentally measured potentials.

There remains the question of the reaction stage at which deprotonation occurs (since the overall reaction from Ph_2NH to DMB^{2+} involves the loss of one proton per Ph_2NH). Rapid deprotonation of $Ph_2NH^{\cdot+}$ followed by coupling of two radicals ($Ph_2N^{\cdot}$) in the rate-determining step would also follow the R–R mechanism. However we favor loss of protons after coupling, since the analogous blocked amine, whose CV is shown in Fig. 4, shows no evidence for proton loss, even with the addition of water. However, deprotonation of the radical cation may occur in the presence of a stronger base, leading to other coupling products (e.g., C–N) and polymer structures.

Relevance to Ph_2NH polymerization

Previous studies of Ph_2NH electrochemical oxidation in MeCN have shown formation of a polymer (poly-diphenylamine) [25—27]. There is good evidence [26,27] that this occurs predominantly (or exclusively) by a C–C (or "tail-to-tail") coupling mechanism to yield a polymer of structure

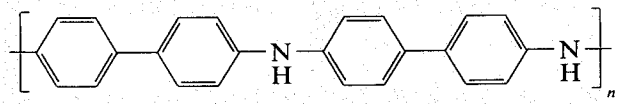

This can be contrasted to the oxidation of aniline, where polyaniline (PA) formation occurs via C–N (or "head-to-tail" coupling [7]. One can also contrast the behavior of these two systems by considering the oxidation of the dimers. As shown above, electro-oxidation of DPB apparently does not lead to the polymer, whereas oxidation of benzidene produces PA [47]. Further studies on the electrochemical oxidation of substituted aromatic amines are in progress.

CONCLUSIONS

Cyclic voltammetry with ultramicroelectrodes is an effective method for the investigation of the initial steps in the electropolymerization of Ph_2NH. The reduction wave of the $Ph_2NH^{\cdot+}$ radical cation was observed at scan rates higher than 100 V/s. The electrogenerated $Ph_2NH^{\cdot+}$ cation undergoes a second-order radical cation-radical cation coupling to form N,N'-diphenylbenzidine (DPB), which then is oxidized to DPB^{2+}, in an EC_2EE reaction pathway. The rate constant of the coupling reaction is 2.0 $(\pm 0.5) \times 10^5$ M^{-1} s^{-1}. In very dry acetonitrile, the parent monomer, Ph_2NH, acts as a proton acceptor. However the presence of a small quantity of water displaces Ph_2NH as the base, and simplifies interpretation of the voltammetry. Under these conditions, the net faradaic charge passed during the electrode reaction is two electrons per Ph_2NH monomer.

ACKNOWLEDGEMENTS

The support of this research by the National Science Foundation (NSF CHE89011450) is gratefully acknowledged. The authors would like to thank the University of Texas System Center for High Performance Computing for providing the necessary computing resources. We also thank Yaw Obeng and Marye A. Fox for helpful discussions, and Dr. Hugh Horowitz for suggesting the study of Vanlube 81.

APPENDIX DETAILS OF DIGITAL SIMULATIONS AND THE $E_p - E_{p/2}$ DIAGNOSTIC CRITERION FOR CV IN EC-REACTIONS

Digital simulations

The simulations followed the usual explicit finite difference method with an exponentially expanding grid [48]. Most were carried out on a CDC Cyber 170/750 system, while those for the fastest homogeneous reactions were performed on a Cray XMP computer. For the simulations in the text the rate constant of all heterogeneous electron transfers were usually taken as 1.0 cm/s; in a few cases an arbitrarily large k° (10^{10} cm/s) was taken to test for any effect of heterogeneous kinetics. The rate constant of the coupling reaction, k, and the scan rate, v, were varied to give the reported values of the dimensionless parameter $\lambda = kcRT/Fv$. The number of iterations employed, L, depended upon the value of λ, i.e., $L \geqslant 10\lambda$; L was at least 10^4 for a single sweep direction, with the largest L being 3.6×10^5.

$E_p - E_{p/2}$ diagnostic criterion

We suggested in the text that the shape of the CV wave, represented by the value of $E_p - E_{p/2}$, is useful in distinguishing among different reaction mechanisms. To demonstrate this, we consider here three simple EC-type mechanisms; for completeness, and to confirm the correctness of the simulations, we also show the usual diagnostic criteria of variation of current function and peak position with λ. The mechanisms discussed here are:

(I) Following first-order reaction

$$\begin{array}{ll} R \rightleftharpoons O + e^- & E \\ O \rightarrow Y & C_1 \end{array}$$

(II) Following product coupling reaction

$$\begin{array}{ll} R \rightleftharpoons O + e^- & E \\ 2\,O \rightarrow Y & C_2 \end{array}$$

(III) Following product–parent coupling reaction

$$\begin{array}{ll} R \rightleftharpoons O + e^- & E \\ R + O \rightarrow Y & C_2' \end{array}$$

In these simulations we assumed that the electron transfer step was totally reversible, and the diffusion coefficients of all species were identical. In this case, no heterogeneous kinetics were involved and the Nernst equation was used as a boundary condition on the electrode surface.

Scheme (I) is the well-known EC reaction [25,38] and is included for comparison to the other schemes. Figures A1, A2, and A3 represent the characteristic variations of peak current, peak potential, and the difference between peak and half-peak potentials vs. log λ, respectively. For scheme (I), $\lambda = k(RT/Fv)$, and for schemes (II) and (III) $\lambda = kc^0(RT/Fv)$. It is convenient to use the zone diagram approach introduced by Savéant and his coworkers [24,43–46,49]. As shown in Figs. A1–A3, there are three zones: the pure diffusion zone, DP, the pure kinetic zone, KP, and the zone where both diffusional and kinetic contributions are present, KO. The boundaries between these zones were established by taking the first peak potential as the criterion for the detection of the diffusional or kinetic character in Fig. A2 [49]. We take the boundary at the pure diffusion (DP) region where the peak potential deviates by 3 mV from the theoretical constant value of $|E_p - E^{0\prime}|$ of 28.50 mV [24]. The boundary at the pure kinetic (KP) region is taken as a 3 mV shift from the line defining the KP behavior.

In the KP zone of Fig. A1, a big difference is observed in the first oxidation peak current. Note that n_{app} for the overall reaction in scheme (III) is 0.5, but is 1 in schemes (I) and (II). In schemes (I) and (II), the oxidation product is consumed by a chemical reaction, which favors diffusion of R to the electrode surface so that the peak current is slightly larger than that of the reversible case. Figure A2 shows that the first peak potentials of all three schemes shift in the negative direction for oxidations in the KP zone. However, the slopes, $\partial(E_p)/\partial(\log \lambda)$, are different. A

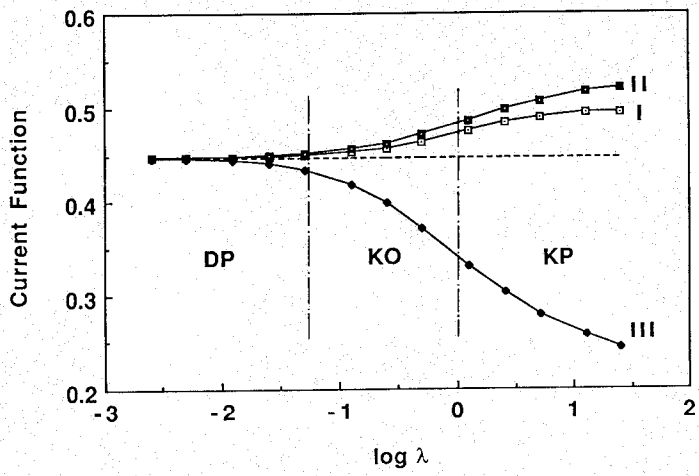

Fig. A1. Simulation of variation of the current function of the first peak vs. log λ. Scheme (I) ▣, (II) ◘, (III) ◆. Dashed line is for Nernstian case.

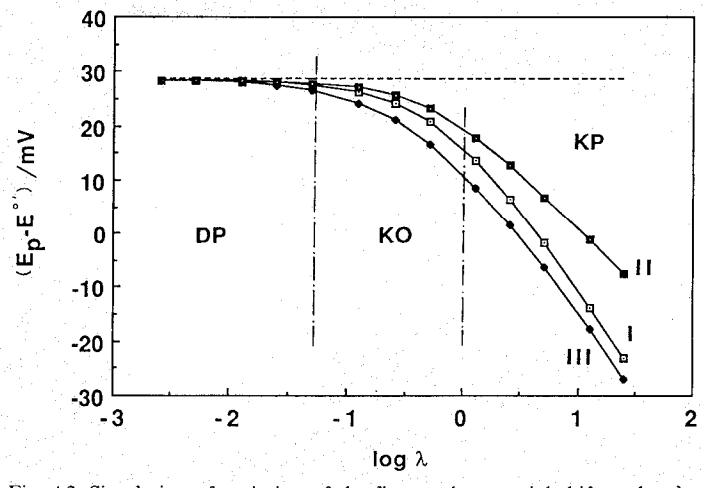

Fig. A2. Simulation of variation of the first peak potential shift vs. log λ. (I), ▣, (II) ◘, (III) ◆. Dashed line is for Nernstian case.

negative shift of about 30 mV is observed for a ten-fold increase in λ for scheme (I). The same behavior is observed in scheme (III) (i.e., as in the product–parent coupling mechanism), the slope is the same as that in scheme (I) and the peak potential shift is larger than scheme (I). The peak potential shift for scheme (II) is smaller than schemes (I) and (III), with a slope of about 20 mV per tenfold increase in λ. As shown in Fig. A3, the half-peak potential separations ($E_p - E_{p/2}$) of the three schemes in the KP zone are different from one another. The limiting value of

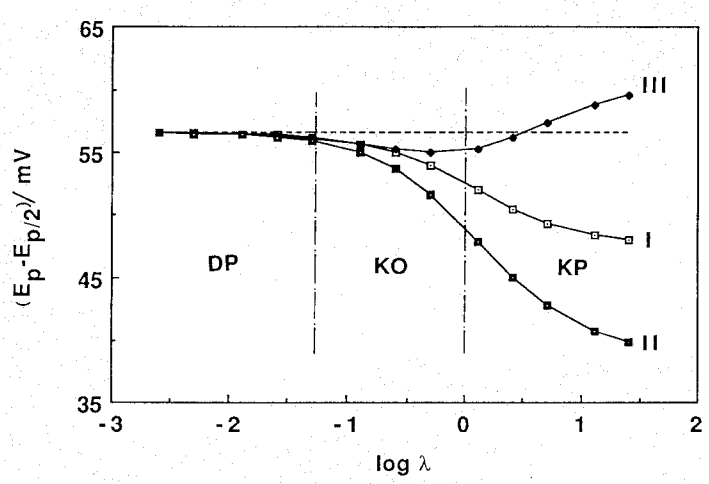

Fig. A3. Simulation of variation of ($E_p - E_{p/2}$) vs. log λ. Scheme (I) □, (II) □, (III) ◆. Dashed line is for Nernstian case.

($E_p - E_{p/2}$) for the product-parent coupling scheme is ca. 58 mV, while it is 40 mV for the product coupling scheme (II), and ca. 50 mV for the first-order EC scheme (I). The variations of $E_p - E_{p/2}$ with log λ are also different, with scheme (III) showing a positive deviation from the reversible value, while schemes (I) and (II) show negative deviations. Of course measurements of $E_p - E_{p/2}$ can be compromised by the presence of uncompensated resistance, but they are unaffected by drift in the reference electrode potential.

REFERENCES

1 R.C. Reed and R.M. Wightman in A.J. Bard and H. Lund (Eds.), Encyclopedia of Electrochemistry of the Elements, Organic Section, Vol. 15: Derivatives of Ammonia Heteroaromatic Compounds, Marcel Dekker, New York, 1984, pp. 1–165.
2 R.F. Nelson in A. Weissberger (Ed.), Techniques of Chemistry, Vol. 5: N.L. Weinberg (Ed.), Technique of Electroorganic Synthesis, Part 1, Wiley, New York, 1974, pp. 535–792.
3 R.N. Adams, Electrochemistry at Solid Electrodes, Marcel Dekker, New York, 1969, pp. 327–356.
4 R.F. Nelson and S.W. Feldberg, J. Phys. Chem., 73 (1969) 2623.
5 A.F. Diaz and J.A. Logan, J. Electroanal. Chem., 111 (1980) 111.
6 R. Noufi and A. Nozik, J. Electrochem. Soc., 129 (1982) 2261.
7 E.M. Genies, A. Boyle, M. Lapkowski and C. Tsintavis, Synth. Met., 36 (1990) 139, and references therein.
8 T. Hagiwara, T. Demura and K. Iwata, Synth. Met., 18 (1987) 317, and references therein.
9 E.T. Seo, R.F. Nelson, J.M. Fritsch, L.S. Marcoux, D.W. Leedy and R.N. Adams, J. Am. Chem. Soc., 88 (1966) 3498.
10 A. Volkov, G. Tourillon, P.-C. Lacaze and J.-E. Dubois, J. Electroanal. Chem., 115 (1980) 279.
11 E.M. Genies and M. Lapkowski, J. Electroanal. Chem., 236 (1987) 189.
12 T. Ohsaka, Y. Ohnuki, N. Oyama, G. Katagiri and K. Kamisako, J. Electroanal. Chem., 161 (1984) 399.
13 G. Zotti, S. Cattarin and N. Commiso, J. Electroanal. Chem., 239 (1988) 387.
14 K. Chiba, T. Ohsaka and N. Oyama, J. Electroanal. Chem., 217 (1987) 239.
15 P. Gao, D. Gosztola and M.J. Weaver, J. Phys. Chem., 93 (1989) 3753.
16 M. Takakubo, J. Electroanal. Chem., 258 (1989) 303.
17 N. Oyama, K. Hirabayashi and T. Ohsaka, Bull. Chem. Soc. Jpn., 59 (1986) 2071.
18 T. Ohsaka, K. Hirabayashi and N. Oyama, Bull. Chem. Soc. Jpn., 59 (1986) 3423.
19 J. Bargon, S. Mohmand and R.J. Waltman, IBM J. Res. Develop., 27 (1983) 330.
20 G. Cauquis, J. Cognard and D. Serve, Electrochim. Acta, 20 (1975) 1011.
21 M. Genies and A.F. Diaz, J. Electroanal. Chem., 98 (1979) 305.
22 N. Vettorazzi, J.J. Silber and L. Sereno, J. Electroanal. Chem., 125 (1981) 459.
23 W.V. Childs, J.T. Maloy, C.P. Keszthelyi and A.J. Bard, J. Electrochem. Soc., 118 (1971) 874.
24 A.J. Bard and L.R. Faulkner, Electrochemical Methods, Wiley, New York, 1974.
25 U. Hayat, P.N. Bartlett, G.H. Dodd and J. Barker, J. Electroanal. Chem., 220 (1987) 287.
26 N. Comisso, S. Daolio, G. Mengoli, R. Salmaso, S. Zecchin and G. Zotti, J. Electroanal. Chem., 255 (1988) 97.
27 J. Guay and Lê H. Dao, J. Electroanal. Chem., 274 (1989) 135.
28 D. Serve, Electrochim. Acta, 21 (1976) 1171.
29 R.L. Hand and R.F. Nelson, J. Electrochem. Soc., 125 (1978) 1059.
30 E.M. Genies, G. Bidan and A.F. Diaz, J. Electrochem. Soc., 149 (1983) 101.
31 T. Mizoguchi and R.N. Adams, J. Am. Chem. Soc., 84 (1962) 2058.
32 Z. Galus and R.N. Adams, J. Am. Chem. Soc., 84 (1962) 2061.
33 E.M. Genies and C. Tsintavis, J. Am. Chem. Soc., 195 (1985) 109.

34 K. Aoki and J. Osteryoung, J. Electroanal. Chem., 122 (1981) 19.
35 K. Aoki and J. Osteryoung, J. Electroanal. Chem., 160 (1984) 335.
36 D. Shoup and A. Szabo, J. Electroanal. Chem., 140 (1982) 137.
37 D.O. Wipf and R.M. Wightman in A.J. Bard (Ed.), Electroanalytical Chemistry, Vol. 15, Marcel Dekker, New York, 1989, pp. 267–353.
38 R.S. Nicholson and I. Shain, Anal. Chem., 36 (1964) 706.
39 R.S. Nicholson and I. Shain, Anal. Chem., 37 (1965) 178.
40 W.M. Schwarz and I. Shain, J. Phys. Chem., 69 (1965) 30.
41 D.O. Wipf, A.C. Michael and R.M. Wightman, J. Electroanal. Chem., 269 (1989) 15.
42 D.O. Wipf and R.M. Wightman, J. Phys. Chem., 93 (1989) 4286.
43 C.P. Andrieux, P. Hapiot and J.-M.Savéant, J. Phys. Chem., 92 (1988) 5987.
44 P. Hapiot, J. Moiroux and J.-M. Savéant, J. Am. Chem. Soc., 112 (1990) 1337.
45 L. Nadjo and J.-M. Savéant, J. Electroanal. Chem., 48 (1973) 113.
46 M. Gareil and J.-M. Savéant, J. Electroanal. Chem., 147 (1983) 1.
47 Y. Wei, G.-W. Jang, C.-C. Chan, K.F. Hsueh, R. Hariharan, S.A. Patel and C.K. Whitecar, J. Phys. Chem., 94 (1990) 7716.
48 S.W. Feldberg, J. Electroanal. Chem., 127 (1981) 1.
49 J.-M. Savéant and E. Vianello, Electrochim. Acta, 8 (1963) 905.